

Effect of rinsing temperature on electrical characteristics of ZnO TFTs built using successive ionic layer adsorption and reaction

P.-Y. LEE, S.-P. CHANG*, H.-H. LIN, S.-J. CHANG

*Institute of Microelectronics and Department of Electrical Engineering,
Center for Micro/Nano Science and Technology, Advanced Optoelectronic Technology
Center, National Cheng Kung University, Tainan 70101, Taiwan*

In this study, the effects of ethylene glycol treatment temperature on the transfer characteristics of ZnO thin film transistors (TFTs), constructed using successive ionic layer adsorption and reaction (SILAR), were investigated. Under high-temperature solution treatments, the TFT device demonstrated the typical positive shift in threshold voltage (ΔV_{th}). The shifting phenomenon results from lower oxygen vacancies attributable to $Zn(OH)_2$ in the films following a rise in the treatment temperature. However, at temperatures higher than 145°C, particle mobility tends to be significantly reduced due to the shedding of ZnO from the surface. As a result, the influence of treatment temperature on SILAR is an essential topic of study.

(Received March 19, 2014; accepted January 21, 2015)

Keywords: Zinc oxide, Thin film transistor, Successive ionic layer adsorption and reaction, Temperature treatment

1. Introduction

Zinc oxide is a direct bandgap semiconductor used in many applications [1-9]. It also has potential applications in ultra-violet LED, sensor, and related laser devices [10-12]. It also offers advantages such as low cost, high resource availability, stability in hydrogen plasma and non-toxicity. ZnO-TFTs have attracted a lot of attention because of their potential use as active-matrix liquid crystal display (AMLCD) switching devices. The higher mobility of ZnO-TFTs is suitable for 3D and high-resolution large-area displays. A number of techniques have been employed for fabricating ZnO thin films for application as the active layer in TFTs, such as chemical vapor deposition, sol-gel, spray-pyrolysis, molecular beam epitaxy, pulsed laser deposition, vacuum arc deposition, SILAR and magnetron sputtering [13-23]. Among them, SILAR is the most promising one for the deposition of transparent oxide, because of the high reliability and low cost. Besides, it only requires a low temperature environment and facilitates large-area deposition. Even though there are studies for the differences among various rising procedures involving the use of ethylene, there are very few studies investigating the effect of temperature treatment in ethylene glycol.

In the present study, ZnO thin films with different rising temperatures were prepared using the SILAR method, and structural, optical properties affected by temperature treatment were investigated. Moreover, ZnO-channel TFTs were fabricated and their electrical characteristics were evaluated at different temperatures.

2. Experiment

Inverted staggered-structure TFTs were fabricated on a glass substrate. A 100 nm-thick Al gate electrode was deposited using thermal evaporation and patterned using a metal mask. A dielectric layer of 200 nm-thick SiO_2 was subsequently deposited using plasma-enhanced chemical vapor deposition (PECVD). The active layer was fabricated by depositing a 100 nm-thick ZnO film using the successive ionic layer adsorption and reaction method. $ZnCl_2$ (0.1 M) and concentrated ammonium hydroxide (NH_4OH ; 29wt% NH_3) were used to prepare a tetraammonium zinc complex ($[Zn(NH_3)_4]^{2+}$) solution. NH_4OH was added to adjust the pH of the solution to 10. ZnO film growth was performed, through 20 deposition cycles, and then the crystallinity and microstructure of the films were studied. During the active layer deposition, the temperature of ethylene glycol was set to 95, 125, and 165°C to convert $Zn(OH)_2$ to ZnO [15]. A 100 nm-thick Al layer was deposited using thermal evaporation and patterned as source and drain electrodes. The channel dimensions of the studied TFTs were $L = 200 \mu m$ and $W = 2000 \mu m$.

The structure and crystallite size of the deposited films were investigated using X-ray diffraction (XRD). The surface morphologies of the samples were examined using scanning electron microscopy (SEM) and atomic force microscopy (AFM). The optical properties of the ZnO thin films were characterized by ultraviolet-visible-near-infrared (UV-vis-IR) spectrophotometry, photoluminescence (PL) spectroscopy, and X-ray photoemission spectroscopy (XPS). All electrical

characteristics were measured using an Agilent B1500A semiconductor device parameter analyzer.

3. Result and Discussion

Fig. 1 shows the XRD patterns of the ZnO thin films; the patterns observed after rinsing with ethylene glycol at 95°C, 125°C and 165°C were observed to have wurtzite structure with a preferred c-axis orientation of (002) at $2\theta = 34^\circ$. Peaks due to the (101) plane of wurtzite ZnO were also found, while the peaks were reduced with

increasing temperatures. However, the (002) peak has an obvious increase as the temperature rises to 165°C. Besides, the diffraction angle of the ZnO was increased, indicating better crystallinity with more relaxation. This was the consequence of higher treatment temperatures of the ethylene glycol in the ZnO crystal. Moreover, the full widths at half maximums (FWHM) of ZnO films reduced as T_{ris} increased, possibly due to the increased grain sizes. The grain size for the as-grown sample at 95°C, 125°C and 165°C was 41.9, 47.1, and 50.8nm, these consequences demonstrate that the quality of ZnO thin films depends on temperature.

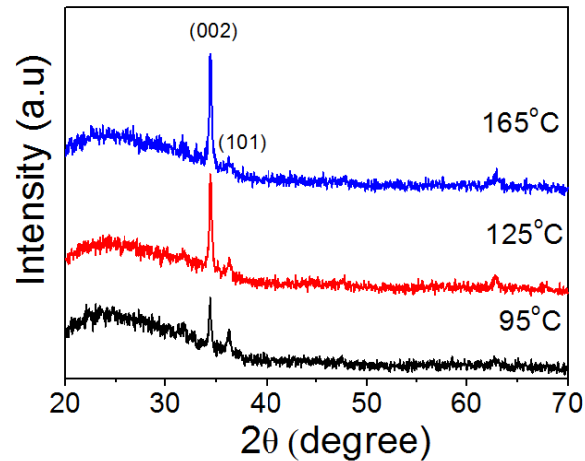


Fig. 1 XRD patterns of ZnO thin films under various temperature treatments

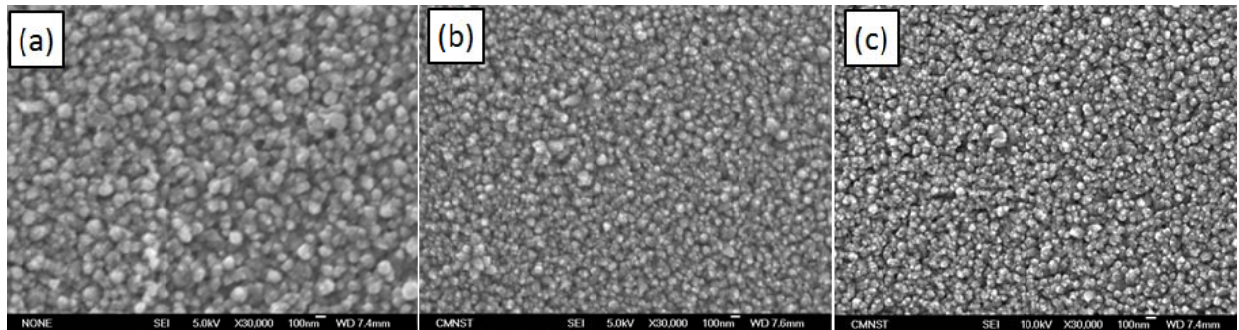


Fig. 2 SEM surface image of the ZnO channel layer at temperatures of (a) 95°C, (b) 125°C, and (c) 165°C

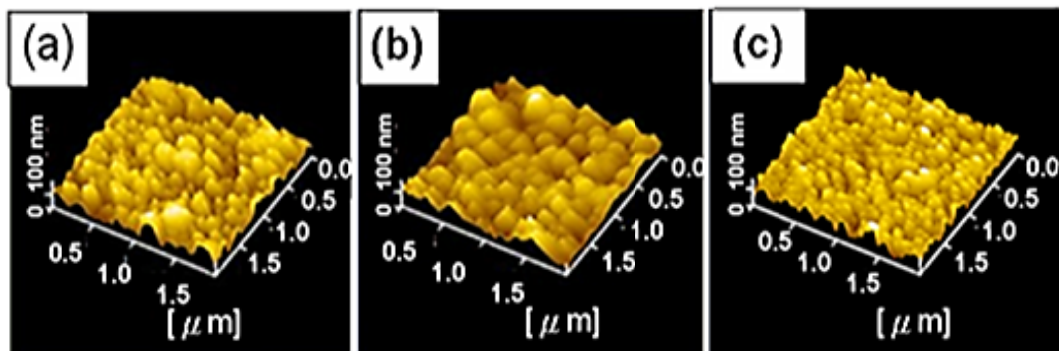


Fig. 3 AFM image of the ZnO channel layer at temperatures of (a) 95°C (b) 125°C, and (c) 165°C

Fig. 2 (a)-(c) shows the evolution of the surface morphologies of ZnO films deposited at different temperatures. It is clear that when the temperature is high, grain size becomes smaller and the surface of the film is smooth and dense without macroscopic defects. When the temperature is below 95 °C, obvious grain boundaries and macroscopic defects begin to emerge. These results indicate that the rinsing temperature evidently affects the structural properties of the films, which can be more compact at higher temperatures. The effect of treatment temperature was also confirmed with AFM images. Figure 3 shows the morphologies of ZnO deposited at various temperatures. The morphology of ZnO films becomes poor and rough with lower film density as rinsing temperature decreases. Increasing the treatment temperature of ethylene glycol reduces surface smoothness as a result of better dispersion. In ethylene glycol, higher temperatures are necessary to break the intra-molecular hydrogen bonds. During the ethylene glycol rinsing procedures, an open monomeric structure is preferred for interacting with the hydroxyl groups absorbed at the ZnO surface. Binding prevents water molecules from getting on the ZnO surface and results in the dispersion of ZnO particles [24]. As a result, higher temperatures are necessary to obtain compact films.

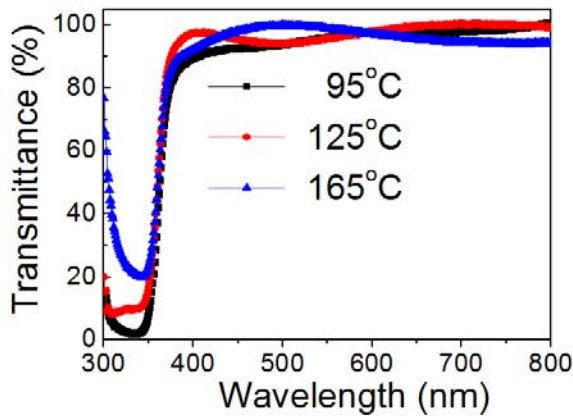


Fig. 4 The optical transmittance spectra at different rinsing temperatures

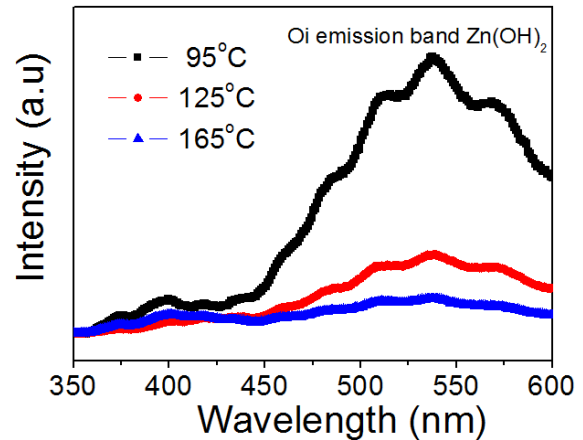


Fig. 5 The PL spectra at different rinsing temperatures

The transmittance spectra of the films deposited at rinsing temperatures of 95°C, 125°C, 165°C are illustrated in Fig. 4. The films are highly transparent in the visible wavelength region. The transmittance increases with increasing treatment temperature. The decrease of transmittance is due to dispersion at the opaque-grain boundaries. In addition, a sharp absorption edge is observed at around 360 nm for all the films.

Fig. 5 shows the PL spectra of films measured at different deposition temperatures. All the samples have two prominent peaks. It is well known that the near-band-edge emission, at about 380 nm, originates from the radiative recombination process in ZnO. The broad peak corresponding to the emission in the green to yellow region is associated with intrinsic deep-level defects in ZnO, such as interstitial oxygen (O_i) and antisite oxygen (O_{Zn}) [25]. In addition, the luminescence band in the range 442–620 nm is attributed to the presence of $Zn(OH)_2$ in the ZnO thin film. $Zn(OH)_2$ is the cause of the O_i emission band (543 nm) [26]. As a result, the spectra indicate that the concentration of O_i in ZnO films increases at low temperatures due to the lack of hydrolysis.

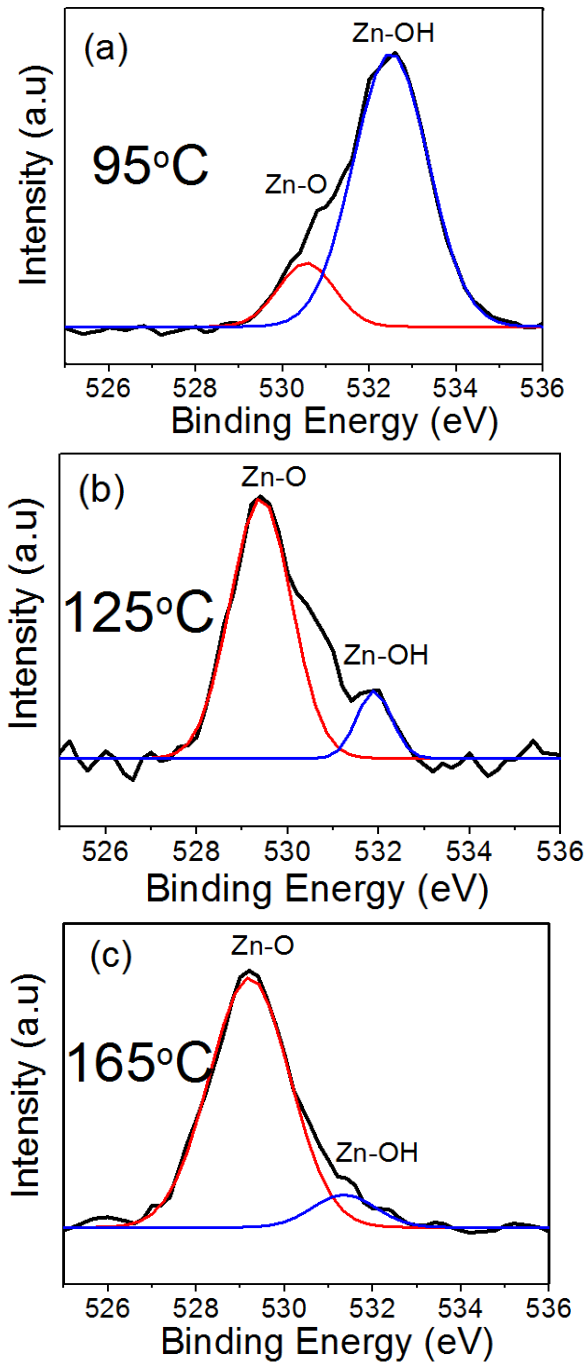


Fig. 6 ZnO XPS spectra of the O 1s of the deposited films at temperatures: (a) 95°C, (b) 125°C, and (c) 165°C

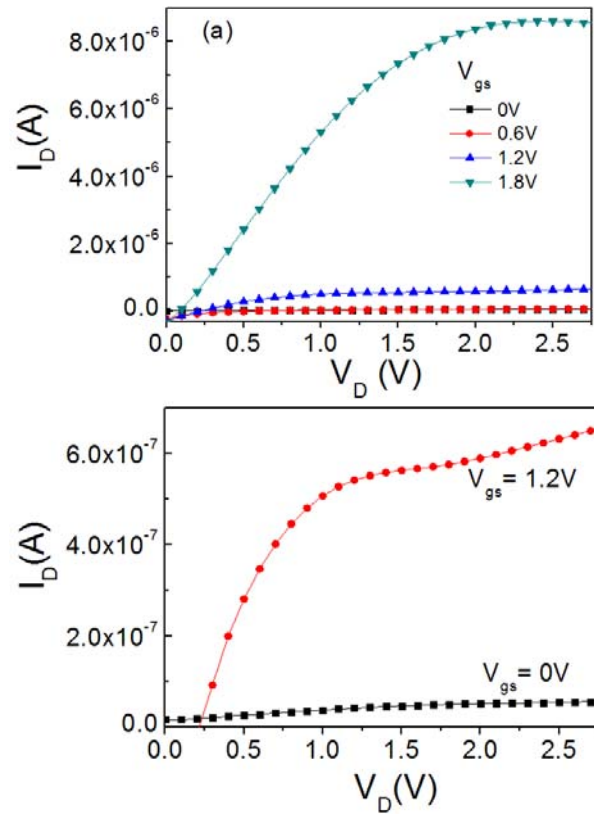


Fig. 7. Output characteristics of SILAR ZnO TFT at (a) 95°C, (b) 125°C

To confirm the effect between the hydrolysis of $Zn(OH)_2$ and rising temperatures, the XPS analysis is presented. An in-depth analysis was performed and the samples were etched more than 50 nm-deep using an Ar ion beam. Figure 6 shows the O 1s spectra of as-grown ZnO films, deposited at various temperatures. The O 1s signals for ZnO films containing O are de-convoluted in two overlapping peaks. The peaks at 530 eV and 532 eV can reasonably be attributed to O^{2-} in Zn-O and Zn-OH, respectively, based on values reported elsewhere [27-28]. At 95 °C, excess $Zn(OH)_2$ that exists in the ZnO film causes high-intensity Zn-OH peaks and low-intensity Zn-O bonding. These results indicate that the films were deficient of oxygen at lower temperatures. However, when the film is rinsed at a higher temperature, the condition could be reversed because of the decomposition of $Zn(OH)_2$. Thus, it can be inferred that the PL and XPS results for the ZnO thin films prepared by SILAR are strongly dependent on the treatment temperature.

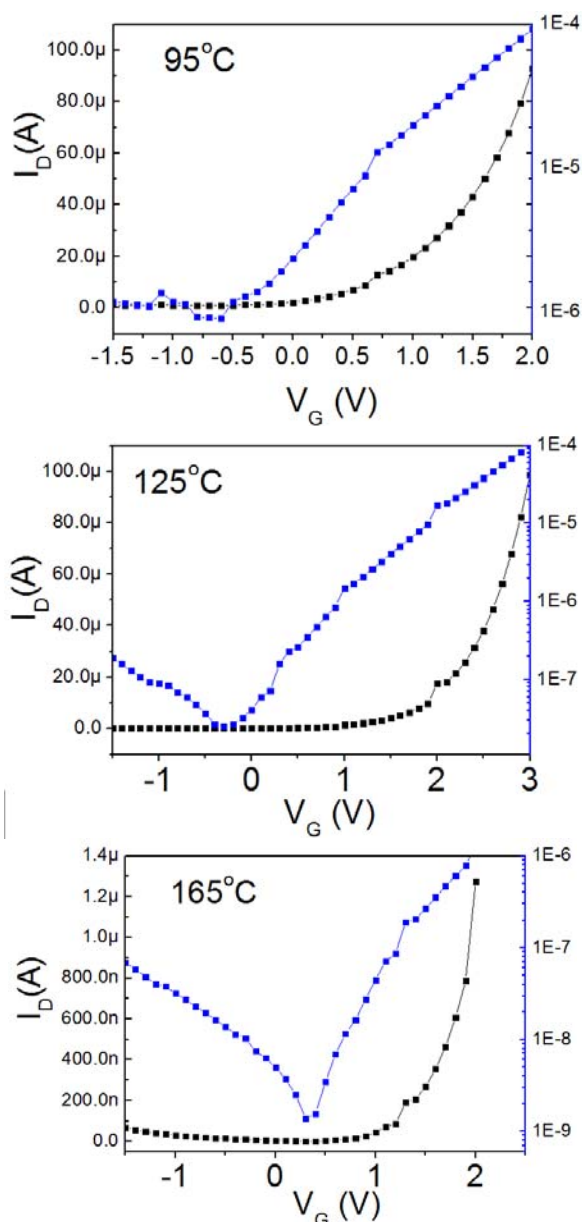


Fig. 8 Transfer characteristics of SILAR ZnO TFT at various temperatures

Table.1 TFT characteristics with various chemical depositions

Method	Sol-gel method [29]	Chemical bath [30]	CVD [31]	Aqueous solution growth [32]	SILAR present work
Mobility (cm ² /Vs)	0.67	3.5	15	0.56	47.8
I _{on} /I _{off} ratio	10 ⁶	10 ⁵	10 ⁷	10 ⁴	10 ⁴

The electrical characteristics of the devices demonstrate that all ZnO TFTs, operated in n-type enhancement mode, require a positive gate voltage to turn on. Figure 7 shows the representative output

characteristics of ZnO under a treatment of 125 °C. The I_D curve is flat for large V_D and hard saturation was observed. The TFTs with ZnO rinsing at 95 °C and 125 °C show similar mobility ~47.8 cm²/Vs, on/off ratio ~10⁴, and SS ~0.9 V/decade. It should be noted that the mobility of ZnO-TFTs, deposited using the SILAR method, is higher than other chemical-processed TFTs shown as Table 1. However, the behavior of the threshold voltage shift under rising temperatures is shown in Fig. 8 (a)-(c). As the temperature increases, the threshold voltage tends to move towards a positive voltage. This phenomenon could be attributed to the reduction at higher rinsing temperatures of oxygen defects, recognized as donors. The results highly correspond to the PL and XPS spectra. However, when the treatment temperature rises to 165°C, the mobility is dramatically reduced to 10.41 cm²/Vs. This probably causes shedding of the ZnO thin films, as the temperature rises. Thus, it can be concluded that the quality of the TFTs, and the structural and optical properties of the thin films depend strongly on the treatment temperature.

4. Conclusion

In summary, the effect of treatment temperature in SILAR-deposited ZnO-TFTs was investigated. Data from PL and XPS have revealed that a temperature rise during ethylene glycol rinsing directly affects the distribution of defects in the films. At low temperatures, the presence of a large number of these defects is attributed to the presence of Zn(OH)₂ in the films, thus affecting the threshold voltage, a TFT transfer characteristic. During the rise in temperature, the threshold voltage increases as a consequence of the reduction in oxygen, which acts as a donor-like defect. As a result, it can be inferred that the properties of ZnO films and ZnO-TFTs are highly dependent on treatment temperature in the SILAR method.

Acknowledgements

This work was supported by the Ministry of Science and Technology under contract number MOST 103-2221-E-006-098 and MOST 103-2622-E-006-042-CC3. This work was also supported in part by the Center for Frontier Materials and Micro/Nano Science and Technology, National Cheng Kung University, Taiwan, and by the Advanced Optoelectronic Technology Center, National Cheng Kung University, under projects from the Ministry of Education.

References

- [1] G. S. Kino, R. S. Wagers, J. Appl. Phys. **44**, 1480 (1973).
- [2] A. O. Maldonado, M. D. L. L. so moza, R. Tirado-Guerra, S., J. Vac. Sci. Technol. A **18**, 2098 (2000).

- [3] H. J. L. Michel, H. Schierbaum, K. D. Halbritter, *Appl. Surf. Sci.* **126**, 57 (1998).
- [4] B. B. Rao, *Mater. Chem. Phys.* **64**, 62 (2000).
- [5] B. D. Sang, K. Yamada, A. Konagai, *Jpn. J. Appl. Phys.* **38**, 4983 (1999).
- [6] Y. P. Wang, W. I. Lee and T. Y. Tseng, *Appl. Phys. Lett.* **69**, 1807 (1996).
- [7] S. Mandal, S. K. Lahiri, A. Dhar, S. K. Ray, *Nanosci. Nanotechnol. Lett.* **1**, 57 (2009).
- [8] W. Water, T. H. Fang, Y. J. Hsiao, L. W. Ji, J. H. Tsai, C. C. Lee, *Nanosci. Nanotechnol. Lett.* **3**, 468 (2011).
- [9] Ch. V. V. Ramana, M. K. Moodley, A. B. V. Kiran Kumar, A. Maity, V. V. Srinivasu, *Nanosci. Nanotechnol. Lett.* **4**, 1203 (2012).
- [10] S. Choopun, R. D. Vispute, W. Noch, A. Balsamo, R. P. Sharma, T. Venkatesan, A. Iliadis, D. C. Look, *Appl. Phys. Lett.* **75**, 3947 (1999).
- [11] A. P. Nayak, T. C. Lin, D. Lam, S. Kaya, M. S. Islam, *Nanosci. Nanotechnol. Lett.* **4**, 977 (2012).
- [12] CH. V. V. Ramana, M. K. Moodley, V. Kannan, *Nanosci. Nanotechnol. Lett.* **6**, 238 (2014).
- [13] B. S. Li, Y. C. Liu, Z. S. Chu, D. Z. Shen, Y. M. Lu, J. Y. Zhang and X. W. Fan, *J. Appl. Phys.* **91**, 501 (2002).
- [14] M. J. Alam, D. C. Cameron, *J. Vac. Sci. Technol. A* **19**, 1642 (2001).
- [15] A. J. C. Fiddes, K. Durose, A. W. Brinkman, J. Woods, P. D. Coates and A. J. Banister, *J. Cryst. Growth* **159**, 210 (1996).
- [16] T. Ohgaki, N. Ohashi, H. Kakemoto, S. Wada, Y. Adachi, H. Haneda and T. Tsurumi, *J. Appl. Phys.* **93**, 1961 (2003).
- [17] Y. R. Ryu, S. Zhu, J. D. Budai, H. R. Chandrasekhar, P. F. Miceli H. W. White, *J. Appl. Phys.* **88**, 201 (2000).
- [18] T. Minami, S. Ida and T. Miyata, *Thin Solid Films* **416**, 92 (2002).
- [19] K. H. Kim, K. C. Park, D. Y. Ma, *J. Appl. Phys.* **81**, 7764 (1997).
- [20] S. C. Shei, P. Y. Lee, S. J. Chang, *Appl. Surf. Sci.* **258**, 8109 (2012).
- [21] P. Pattanaik, S. K. Kamilla, J. Mohapatra, B. K. Jena, D. P. Das, D. K. Mishra, *Nanosci. Nanotechnol. Lett.* **6**, 216 (2014).
- [22] A. A. Tahir, T. D. Smith, and K. G. U. Wijayantha, *Nanosci. Nanotechnol. Lett.* **3**, 674 (2011).
- [23] J. Mohapatra, P. K. Mishra, S. K. Singh, D. K. Mishra, *Nanosci. Nanotechnol. Lett.* **2**, 30 (2010).
- [24] V. Crupi, D. Majolino, P. Migliardo V. Venuti, *Mol. Phys.* **98**, 1589 (2000).
- [25] Y. Hou, M. Yang, G. Pang and S. Feng, *Cryst. Res. Technol.* **42**, 1068 (2007).
- [26] H. Zhou, H. Alves, D. M. Hofmann, W. Kriegseis, B. K. Meyer, G. Kaczmarczyk, A. Hoffmann, *Appl. Phys. Lett.* **80**, 210 (2002).
- [27] N. Takamori, K. Tsujino M. Matsumura, *Jpn. J. Appl. Phys.* **46**, 2944 (2007).
- [28] L. Jing, Z. Xu, J. Shang, X. Sun, W. Cai, H. Guo, *Mater. Sci. Eng. A-Struct. Mater. Prop. Microstruct. Process.* **332**, 356 (2002).
- [29] H. C. Cheng, C. F. Chen and C. Y. Tsay, *Appl. Phys. Lett.* **90**, (2007).
- [30] D. Redinger, V. Subramanian, *IEEE Trans. Electron Devices* **54**, 1301 (2007).
- [31] Jungyol Jo, Ogweon Seo¹, Hyoshik Choi, Byeonggon Lee, *Appl. Phys. Express* **1**, 041202 (2008).
- [32] C. Li, Y. Li, Y. Wu, B. S. Ong and R. O. Loutfy, *J. Appl. Phys.* **102**, 076101 (2007).

*Corresponding author: changsp@mail.ncku.edu.tw